We are IntechOpen,
the world's leading publisher of
Open Access books
Built by scientists, for scientists

6,900
Open access books available

186,000
International authors and editors

200M
Downloads

154
Countries delivered to

Our authors are among the

TOP 1%
most cited scientists

12.2%
Contributors from top 500 universities

CLARIVATE ANALYTICS

BOOK CITATION INDEX

INDEXED

WEB OF SCIENCE™

Selection of our books indexed in the Book Citation Index
in Web of Science™ Core Collection (BKCI)

Interested in publishing with us?
Contact book.department@intechopen.com

Position-Free Vital Sign Monitoring: Measurements and Processing

Dany Obeid, Sarah Samad, Sawsan Sadek,
Gheorghe Zaharia and Ghaïs El Zein

Additional information is available at the end of the chapter

Abstract

As traditional electrodes are perturbing for patients in critical cases such as for burn victims or newborn infants, and even to detect life sign under rubble, a contactless monitoring system for the life signs is a necessity. The aim of this chapter is to present a complete process used in detecting cardiopulmonary activities. This includes a microwave Doppler radar system that detects the body wall motion and signal processing techniques in order to extract the heartbeat rate. Measurements are performed at different positions simultaneously with a PC-based electrocardiogram (ECG). For a distance of 1 m between the subject and the antennas, measurements are performed for breathing subject at four positions: front, back, left, and right. Discrete wavelet transform is used to extract the heartbeat signal from the cardiopulmonary signal. The proposed system and signal processing techniques show high accuracy in detecting the cardiopulmonary signals and extracting the heartbeat rate.

Keywords: Doppler radar, cardiopulmonary signals, wavelet transforms, electrocardiogram, contactless monitoring

1. Introduction

Traditional electrocardiogram (ECG) with affixed electrodes could be perturbing for patients with conditions such as burn victims or newly born infants, or when long duration monitoring is needed. In addition, a monitoring system detecting life signs under rubble or snow is helpful, especially after earthquakes where the detection of life signs over long distance is needed. The utility of microwave Doppler radar used in the detection of life signs has recently in-

creased. Hence, a touchless cardiopulmonary monitoring is needed for such applications and could be a prominent tool in home health care applications.

When a radio wave is transmitted toward a person, it will be reflected off his/her body. If the reflection occurs off the chest of a motionless person, the reflected signal has a phase modulation due to the Doppler effect due to the movement of the chest, which is caused mainly by heartbeats and breathing. On the other hand, when the breath is held, the reflected signal will depend on the chest displacement due to heartbeat alone.

The aim of this chapter is to present a tunable system in terms of power and frequency that shows the capability to detect chest displacement due to heart beat at different operational frequencies and for different transmitted powers. This allows specifying the appropriate operational frequency for the minimum transmitted power. In addition, simultaneously with a PC-based ECG, measurements are performed at the four different sides (front, back, left, and right) of the person under test (PUT). Wavelet transforms are used in order to separate the heartbeat signal from the cardiopulmonary signal and to extract the heartbeat rate (HR).

The rest of this chapter is organized as follows: Section 2 provides background information about chest-wall displacement. Section 3 describes related work for the system design and the signal processing technique. Section 4 presents the proposed system and some preliminary results obtained at different operational frequencies. Section 5 shows the cardiopulmonary signals obtained at different sides from the subject and presents the results upon applying the proposed signal processing technique. Section 6 concludes the work.

2. Chest displacement due to breathing and heart beating

Using microwave Doppler radar, several techniques were established in order to sense the cardiopulmonary activity. When a microwave signal is transmitted to a person's chest, the power of the reflected signal when it occurs at the air/skin interface is higher than the power of the signal reflected from internal organs. Then, the signal reflected off the person's chest contains information about the chest displacement due to cardiopulmonary activity including breathing and heartbeat. Based on these displacements, the heartbeat rate and the respiration rate can be extracted. However, these motions are not the same for all people. This section describes the mechanism of the chest displacement due to both heartbeat and respiration, as well as some experiments measuring the displacement amount.

2.1. Surface motion due to the cardiac cycle

When the heart beats, it pushes blood through the lungs and to tissues throughout the whole body. A pressure is generated when the heart contracts in order to drive the flow of the blood. While contracting, the heart hits the cavity of the chest creating a significant displacement at the surface of the skin. As the left ventricle carries out blood to all parts of the body, the contraction and relaxation of the left ventricle cause a larger chest motion than other heart actions in healthy subjects. During isovolumetric contraction, the heart normally undergoes a

partial rotation in a counterclockwise direction, causing the lower front part of the left ventricle to strike the front of the chest wall [1]. Also, the left ventricle shortens while contracting, shaping the heart to be more spherical, increasing its diameter, and further adding to the impulse on the chest wall [2]. The peak outward motion of the left ventricular impulse occurs either simultaneously with or just after the opening of the aortic valve. Then the left ventricular apex moves inward [1]. The left ventricular motion causes the chest to pulse outward briefly and the adjacent chest retracts during ventricular ejection [3]. This impulse occurs at the lowest point on the chest where the cardiac beat can be seen, and it is normally above the anatomical apex [4]. Some studies found a second outward movement at the apex: the pre-ejection beat [5]. Many techniques for quantitatively measuring the gross displacement of the chest wall have been applied, including the impulse cardiogram [1], a single-point laser displacement system [6], structured lights and the Moiré effect [7], laser speckle interferometry [8], a capacitance transducer [9], a magnetic displacement sensor [10], and a phonocardiographic microphone [11]. The values of the skin motion due to heartbeat vary between individuals due to physiological difference, age differences, and body shape differences. Since the amount and the speed of the motion of the heart within the chest changes with age, it is expected that the amount of the chest motion due to the heartbeat changes with age. Recent studies found that the expected movement of the mitral valve ahead the heart's long axis is about 1.49 cm at age of 20 with an expected velocity of 7.48 cm/s, and 1.22 cm at age of 84 with an expected velocity of 7.48 cm/s [12]. Another study showed that the displacement of the septum decreases with age, but the displacement of the left lateral wall and the posterior wall of the heart remains constant between ages 49 and 73 [13]. The absolute diastolic displacement of annular sites among children increases significantly with increasing body weight (which is expected since the size of the heart and thorax is increasing), but the percent displacement was inversely proportional to body weight [14]. Although there is no significant change in left ventricular ejection volume with age, the arterial pressure wave varies greatly with age: arterial wall thickness increases, arterial diameter increases, and arterial distensibility decreases [15]. The arterial wall rigidity is expressed as [16]

$$\alpha = 0.421 + 0.0602 \times \text{age} \tag{1}$$

This indicates that pulses will be smaller and more difficult to measure in older subjects. At a pulse, subjects aged between 60 and 70 years have 50% lower variation in the cross-sectional area of the artery than subjects aged between 20 and 30 years [16]. When the variation in the arteries' diameter decreases, the amplitude of the surface skin displacement will decrease. This results in decreasing the signal-to-noise ratio when measuring the pulse using a Doppler radar. In average, the peak-to-peak chest motion in adults due to the heartbeat is about 0.5 mm.

2.2. Surface motion due to respiration

The chest surface motion due to breathing is the combination of the abdominal and rib cage movements. A linear correlation exists between cross-sectional area of the thorax, displacement of the diaphragm, displacement of the rib cage, and lung volume [17]. At the third rib,

the angle of the pump handle changes between 20° and 30°, and the rib radius changes between 10.6 and 10.8 cm. At the seventh rib, the angle of the pump handle changes between 30° and 37°, and the rib radius changes between 1.37 and 1.42 cm [18]. Comparing the chest motion in the front/back, left/right, and up/down directions shows that the largest motions correspond to the sternum and the navel. Sternum moves forward 4.3 mm with inspiration, and the navel which moves forward 4.03 mm with inspiration [19]. The relation between tidal volume and abdominal wall linear displacement is measured using a laser displacement measuring device [20]. An expansion of the abdomen is observed: 4 mm for 400 ml inspiration and 11 mm for 1100 ml inspiration. Also, during spontaneous breathing, an abdominal displacement of 12 mm is observed.

3. Related work

This section presents the related work in both system design and signal processing techniques.

3.1. System design

Since the 1970s [21], microwave Doppler radar has been used in sensing physiological movement. The original work was done with heavy, bulky, and expensive components. However, it was useful for research improvements. During the 1980s, heart and respiration signals were obtained using 10.5 GHz frequency signal. Using a horn antenna placed few centimeters from the subject, the system shows capability to detect cardiopulmonary signals using a 10-mW transmitted power [22]. In 1990, systems operating at 2 and 10 GHz were tested in detecting life signs in victims under clutter. The radiated power varied between 10 and 20 mW [23]. In 1997, heartbeat and respiration signals were detected at a distance of 10 m using 24 GHz frequency system with 30 mW output power and 40 dB antenna gain [24]. In the year 2000, systems operating at 450 and 1150 MHz, with a radiated power around 300 mW, were used to detect life sings in victims under rubble [25]. In 2001, a 1.2-GHz, 70-mW quadrature superheterodyne system was used to detect breathing of a subject under 1.5-m rubble [26]. Operating at 1.6 and 2.4 GHz, direct-conversion Doppler radars have been integrated in 0.25 μm complementary metal-oxide semiconductor (CMOS) and BiCMOS technologies. The output power was estimated to be 6.5 dBm [27]. Heart and respiration activities were detected using a modified Wireless Local Area Network (LAN) Personal Computer Memory Card International Association (PCMCIA) card and a module combining the transmitted and reflected signals [28,29]. The operational power of the system was 35 mW and the distance from the subject was 40 cm. Other systems operating in the Ka-band were described in Ref. [30] using a low-power double-sideband transmission signal. For a distance of 2 m from the subject, and for 16 and 12.5 μW, respectively, the systems showed an accuracy of 80% in detecting the heartbeat rate. Recently in 2006, some measurements were performed in order to detect multiple heartbeats signals [31]. Operating at 2.4 GHz and 1 mW power, the system was able to determine the number of persons in a room. With the same characteristics, another system using single and multiple antennas systems showed the possibility of separating two respiration signals [32]. In 2007, a new study showed the possibility of detecting the presence of a person through a wall using ultra-wideband (UWB) radar [33]. Lately in 2008, some experi-

ments are preformed to detect life signs using a 4–7-GHz band with 1 mW power and around 7 dB antenna gain. This system uses the complex signal demodulation (CSD) and the arctangent demodulation in order to cancel random body movements [34]. In 2009, a system operating at 10 GHz showed the ability to detect the heart and the respiration activity of a person behind a wall.

Recently, a system having two Vivaldi antennas, a Mini-Circuits ZHL-42 power amplifier for the transmission, and a Hittite HMC753 low-noise amplifier in the receiver is proposed [35]. The receiver is composed of a down-converter of a 20-MHz IF band, a mixer, an Agilent signal generator and a band-pass filter, and the received signal is sent to the analog-to-digital converter (ADC). A 60-MHz sampling clock provided by an external clock and synchronized with the field-programmable gate array (FPGA) reference clock for the signal digitization. Then, the sampled data are sent to the FPGA for digital down conversion. Another system composed of two antennas, an oscillator that provides both the receiver's local oscillator and the transmitted signal, and a mixer is presented in [36]. I/Q channel demodulation with calibration method is added to alleviate the null point problem and acquire an accurate phase demodulation result with high linearity. Another system presented in [37] is based on multiple transceivers, and antennas with polarization and frequency multiplexing are used to detect signals from different body orientations.

3.2. Signal processing techniques

In Doppler cardiopulmonary monitoring, the heartbeat and the respiration signals are laid together. Hence, a processing technique is needed in order to determine the characteristics of each signal. The signal processing part includes the separation of the cardiopulmonary signals and the extraction of the heartbeat rate. The amplitude of the respiration signal is much greater than the amplitude of the heartbeat signal. Therefore, the respiration rate can be determined without filtering. On the other hand, determining the heartbeat rate needs a processing technique. At rest, the heartbeat rate varies between 50 and 90 beats per minute [38]; this corresponds to a frequency between 0.83 and 1.5 Hz, respectively. On the other hand, the resting respiration rate varies between 9 and 24 breaths per minute [38]; this corresponds to a frequency between 0.15 and 0.4 Hz. Due to the difference of the frequencies that correspond to the heartbeat and the respiration rates, the average heartbeat rate could be determined upon extracting the frequency components of the cardiopulmonary signals. This allows determining the average heartbeat rate over a specific window of time. On the other hand, determining the heartbeats variation over time needs a peak-finding technique.

Several techniques were used in processing the cardiopulmonary signals. This processing includes separating the heartbeat signal from the respiration signal and then finding the heartbeat rate. Some measurements were performed while holding the breath. This eliminates the isolation process of the heartbeat signal, but a filtering approach is still needed in order to remove noise and distorting signals.

First measurements for heartbeat and respiration were performed separately. Holding the breath allows detecting the heartbeat signal [21]. Another study shows the possibility of measuring the heartbeat and respiration activities successively where a low-pass filter with 4

Hz cutoff frequency was used to remove unwanted frequencies [23]. In 2000, heartbeat and respiration signals were measured simultaneously. The output signal is fed through a band-pass filter (BPF) with passing band between 0.1 and 4 Hz. The heartbeat and respiration rates are obtained by applying fast Fourier transform (FFT) to the original signal. The dominant peak in the frequency domain was taken as the breathing frequency, and the second dominant peak was taken as the heartbeat frequency [25]. In 2002, separated measurements for heartbeat and respiration were performed. The respiration signal was filtered with a BPF (0.03–0.3 Hz), and the heart signal was filtered with a BPF (1–3 Hz) [27]. Another work tended to detect the heartbeat signal using a 12-dB/octave high-pass filtering at 0.03 Hz in order to remove DC offset, and a 12-dB/octave low-pass filtering at 3 Hz was used to avoid aliasing error. The heart signal was further isolated with an additional 12 dB/octave HPF at 1 Hz [39]. Also in 2002, measurements for breathing persons were performed. The respiration signal was isolated using a fourth-order low-pass Butterworth filter with cutoff frequency at 0.7 Hz. The heartbeat signal was isolated using a fourth-order band-pass Butterworth filter with cutoff frequencies at 1 and 3 Hz. The rate determination is based on the use of auto-correlation. A spatial zero-forcing filter is applied so that the DC is removed from the measured received signal [40]. In 2003, a wireless LAN PC card was used. A low-pass resistor-capacitor (RC) filter having a cutoff frequency 100 Hz is used to filter the baseband output of the receiver. This helps denoising the signal as well as avoiding aliasing error. The filtered signal is then converted to digital in order to be processed in a notebook PC. The prefiltered, digitized signal was filtered further in the digital domain to separate the heart and breathing signals. The heart signal was isolated using a 0.75–5 Hz band-pass filter for 10 s interval. Based on the periodicity of the autocorrelation function, the heartbeat rate was estimated [28]. In 2006, a system using a signal processing part similar to some previous work is stated. The heartbeat signal was first separated from the respiration signal by a Butterworth BPF with passband from 0.7 to 3 Hz. The filtered signal was then windowed and auto-correlated. Then, FFT was applied to the auto-correlated signal to obtain the heartbeat rate [41].

Recently, other processing techniques are used for cardiorespiratory separation. In [35], FPGAs are used to process either time- or frequency-domain signals in human sensing radar applications. It is applied for continuous wavelet (CW) and UWB radars. In CW Doppler radar, a novel superheterodyne receiver is used to suppress low-frequency noise and includes a digital down-converter module implemented in an FPGA. In [36], compact quadrature Doppler radar sensor is used: Continuous wavelet filter and ensemble empirical mode decomposition (EEMD) based algorithms are applied for cardiorespiratory signal to separate the cardiac and respiratory signals. The accurate beat-to-beat interval can be acquired in time domain for heart rate variability (HRV) analysis. A curvelet transform is applied in [42] in order to remove the direct coupling wave and background clutters. Life signals are denoised using a singular value decomposition. Both the FFT and the Hilbert-Huang transform are applied in order to separate and extract the frequencies of the human vital sign as well as the characteristics of micro-Doppler shift for an UWB radar. Least mean square adaptive harmonic cancellation algorithm is proposed in [43] to separate the breathing and heartbeat signal from biological Doppler radar. The respiration signal is used as a model reference input while the radar signal due to body motion is considered as the original input of the model. A model is designed and

validated experimentally with commercial motion detector [44]. A low-pass filter with 0.7 Hz cutoff frequency is used to extract the respiration signal, while a band-pass filter between 0.9 and 2.5 Hz is used to extract the heartbeat signal. In [37], complex technique is discussed; a complex signal demodulation technique is proposed to eliminate the null detection point problem in non-contact vital sign detection. This technique is robust against DC offset in a direct conversion system. Hence, a random body movement cancellation technique is developed to cancel out strong noise caused by random body movement in non-contact vital sign monitoring. The complex signal is software reconstructed in real time by $S(t) = I(t) + j Q(t)$. System setup of random body movement cancellation technique is designed of two transceivers, one in front of and the other behind the human body, which are transmitting and receiving signals with different polarization and wavelength. The two complex signals are multiplied. This multiplication corresponds to convolution and frequency shift in frequency domain, thus canceling the Doppler frequency drift and only keeping the periodic Doppler phase effects. In [45], fast acquisition of HR is proposed, the length of the time window is less than 5 s and the accuracy is significantly degraded due to insufficient spectrum resolution. In [37], CSD is used for vital sign detection. A time-window-variation technique is developed for fast acquisition of HR from short-period time windows and measuring HR variation using CSD. The proposed method has also proved to be able to measure HR variation using CSD.

3.3. Discussion

Systems used in these works lack determining the most appropriate parameters for these applications. These parameters are the operational frequency, the radiated power, and the optimal signal processing technique. The proposed system shows the ability of tuning both the operational frequency and transmitted power. Hence, it is able to determine better emitted frequency with less power that detects heartbeat accurately. On the other hand, most of the processing techniques tend to extract an average heartbeat rate of the subject. This does not give information about the variation of the heartbeat rate and requires a long-duration window which makes the real-time processing not possible. The proposed signal processing technique shows the ability to detect the variation of the heart activity in time.

4. Proposed system: design and preliminary results

The most important factors in a Doppler radar using a CW signal are the operational frequency and the radiated power. The former governs the penetration of clothing, the reflection at the air/skin interface, and the signal-to-noise ratio. The latter must be taken into consideration as both patients and medical staff are exposed to the radiations. Our proposed system shows the ability of tuning the operational frequency, as well as the transmitted power. The choice of the operational frequency and the radiated power are subject to international standards.

This section introduces the limitations in terms of power and frequency, presents the proposed system, and shows the preliminary results obtained at different operational frequencies: 2.4, 5.8, 10, 16, and 60 GHz.

4.1. Frequency and power limitations

The touchless cardiopulmonary detection is based on a reflected signal off the person's chest. Hence, the most important feature is that the RF signal penetrates clothing with minimal reflection and has a higher reflection at the air/skin interface. These properties depend on the operational frequency. For most microwave frequencies, the reflection at the air/skin interface is high. However, the signal reflects at the air/skin interface less as the frequency decreases, and it has more significant reflections from clothing or bedding as the frequency increases. As shown in Eq. (3), the amount of the phase variation is indirectly proportional to wavelength of the carrier. Hence, the signal-to-noise ratio is directly proportional to the operational frequency ($f = c/\lambda$). The higher the frequency, the shorter the wavelength, and then the greater the phase variation. For a constant phase noise at different frequencies, increasing the frequency increases the signal-to-noise ratio. Another feature related to the operational frequency is the antenna size. As the frequency increases, the same antenna gain can be obtained with a physically smaller antenna. The maximum directivity that can be obtained from an antenna with aperture area A is

$$D_{\max} = \frac{4\pi A}{\lambda^2} \qquad (2)$$

where λ is the wavelength of the transmitted signal. When λ decreases, the area decreases for constant directivity. All these factors should be taken into consideration in order to specify the operational frequency.

As the Doppler radar results in a transmitted power, it is necessary to decrease the transmitted power in order to decrease the radiated energy the patient is exposed to during measurements. Various organizations and countries have developed exposure standards for radio frequency energy. These standards recommend safe levels of exposure for both the general public and for workers. Since 1985, In the USA, the Federal Communications Commission (FCC) has accepted and used approved safety guidelines for the exposure of the RF environmental. Several Federal health organizations such as the US Food and Drug Administration (FDA), the Environmental Protection Agency (EPA), the Occupational Safety and Health Administration (OSHA), and the National Institute for Occupational Safety and Health (NIOSH) have also been concerned in issues related to monitoring and RF exposure [46]. The FCC guidelines for human exposure to RF electromagnetic fields were derived from the recommendations of two expert organizations: the National Council on Radiation Protection and Measurements (NCRP) and the Institute of Electrical and Electronics Engineers (IEEE). Both the NCRP exposure criteria and the IEEE standard were developed by expert scientists and engineers after extensive reviews of the scientific literature related to RF biological effects.

The exposure guidelines are based on thresholds for known adverse effects, and they incorporate prudent margins of safety. In adopting the most recent RF exposure guidelines, the FCC consulted with the EPA, FDA, OSHA, and NIOSH and obtained their support for the guidelines that the FCC is using. The International Commission on Non-Ionizing Radiation Protec-

tion (ICNIRP) has developed exposure guidelines that are applicable in many countries including Europe. The safety limits stated by the ICNIRP limits are similar to those stated by the NCRP and IEEE, with few exceptions. For example, ICNIRP recommend different exposure thresholds in both the lower and the upper frequency ranges and for localized exposure due to some devices as cellular phones. The NCRP, IEEE, and ICNIRP exposure guidelines identify the same threshold level at which harmful biological effects may occur, and the values for maximum permissible exposure (MPE) recommended for electric and magnetic field strength and power density are based on this level. The American National Standards Institute (ANSI) standard was developed over a period of several years by scientists and engineers with considerable experience and knowledge in the area of RF biological effects and related issues. The recommendations were based on a determination that the threshold of hazardous biological effects was approximately 4 W/kg [47]. The Watts per kilogram unit is an expression for the rate of energy absorption in the body given in terms of the specific absorption rate (SAR). A safety factor of 10 was then incorporated to arrive at the final recommended protection guidelines. In other words, the protection guides can be correlated with an SAR threshold of about 0.4 W/kg [29]. In addition, the guidelines stated by NCRP, IEEE, and ICNIRP for the maximum permissible exposure depend on the transmitting frequencies. This is caused by the fact that the human body absorption of RF energy varies accordingly with the RF signal frequency. The highest RH energy absorbed by the human body lies in the frequency range 30–300 MHz; thus, the most restrictive limits are applied. Other exposure limits are stated for devices that expose only part of the body such as mobile phones [48].

4.2. System operating at different frequencies

The proposed system consists of using only a vector network analyzer (VNA) and two antennas. This accommodates a quick and simple installation process. **Figure 1** represents the proposed system. Beside simplicity, many benefits are offered upon the use of a VNA. This section describes the characteristics of the proposed system including VNA and antennas and shows the benefits of this system.
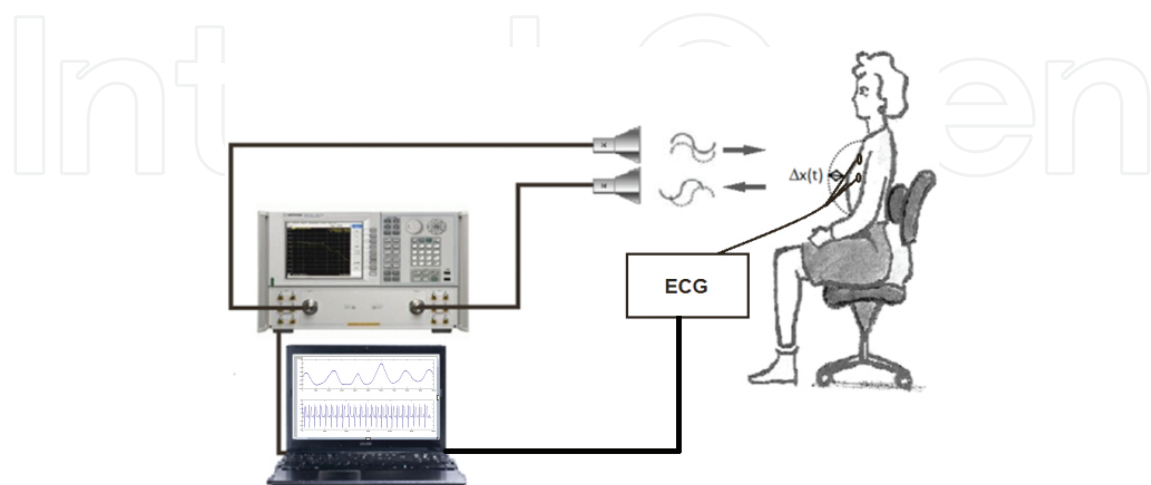

Figure 1. Proposed system design: microwave system and ECG.

In order to provide a comparative study in terms of operational frequency, several frequencies were tested using the proposed system. The operational frequencies should cover as much radar band designations as possible, as well as industrial-scientific-medical (ISM) bands. The operational frequencies chosen in this work are 2.4 GHz (ISM S-band), 5.8 GHz (ISM C-band), 10 GHz (X-band), 16 GHz (Ku-band), and 60 GHz (ISM V-band). Choosing these frequencies allows providing a comparative approach for different frequencies. In addition, the choice of the frequencies covers different bands of frequencies, specifically, S, C, X, Ku, and V bands. Also, the chosen frequencies include within some ISM bands, specifically 2.4, 5.8, and 60 GHz. Besides, these frequencies are selected taking into account the operational limits of the VNA and the antennas.

4.3. Vector network analyzer

VNA is one of the most used systems for microwave measurements and RF applications. It allows verifying the RF performance of microwave devices as well as their characterization in terms of network scattering parameters or S parameters in both magnitude and phase. The utilized vector network analyzer is an HP N5230A 4-port PNA-L. This VNA provides the combination of speed and accuracy for measuring multi-port and balanced components such as filters, duplexer, and RF modules up to 20 GHz. The N5230A VNA provides the following features and benefits:

- Full 4-port S parameter and balanced measurements up to 20 GHz

- 120 dB dynamic range at 20 GHz

- <0.006 dB of trace noise at 100 kHz intermediate frequency band width (IFBW)

- <4 μs/point measurement speed

- Automatic port extension automatically corrects for in-fixture measurements

- Advanced connectivity with LAN, universal serial bus (USB), and general purpose interface bus (GPIB) interfaces

4.4. Antennas

The same wide band antennas (Q-par Angus Ltd.) were used for transmission and reception in experiments performed between 2 and 18 GHz. The Q-par Angus Ltd. (model number WBH2-18HN/S) has a frequency range between 2 and 18 GHz, with a nominal gain between 10 and 22 dBi and a nominal beam width between 6° and 11°. The voltage standing wave ratio (VSWR) of the antenna is less than 2.5:1 (typically <2.0:1), and its cross polar is less than −17 dB. The antenna dimensions are 622 × 165 × 165 mm approximately, it weighs 2.7 kg and operates for temperatures between −40 and +70°C.

4.5. System operating at 60 GHz

In order to provide a comparative approach, an extension to the proposed system is added in order to sustain a frequency signal of 60 GHz. This is achieved using up-conversion and down-

conversion methods. As the operational range of the VNA is limited to 20 GHz, a 3.5 GHz signal is up-converted to 60 GHz, then transmitted. The received 60 GHz signal is down-converted to 3.5 GHz. The measurement system is shown in [49]. The up- and down-conversion processes are obtained as follows: the VNA generates a CW signal at 3.5 GHz. Mixed with the phase locked oscillator (PLO) at 56.5 GHz frequency, the 3.5 GHz frequency is up-converted to 60 GHz. The IF signal is sent to the RF block. This block is composed of a mixer, a frequency tripler, a PLO at 18.83 GHz and a Band-Pass Filter (BPF) (59–61 GHz). The local oscillator (56.5 GHz) frequency is obtained with an 18.83 GHz PLO with 70 MHz external reference and a frequency tripler. The phase noise of the 18.83 GHz PLO signal is about −110 dBc/Hz at 10 kHz off carrier. The Band Pass Filter (BPF) with a bandwidth of 59–61 GHz removes out-of-band spurious signals caused by the modulator operation. The 0-dBm obtained signal is fed into a horn antenna with a gain of 22.4 dBi and a half-power beam width (HPBW) of 10° E and 12° H. The receiving antenna, identical to the transmitting horn antenna, is connected to a BPF (59–61 GHz). The input BPF removes the out-of-band noise. The RF filtered signal is down-converted to an IF signal centered at 3.5 GHz and fed into a BPF with a bandwidth of 2 GHz. A low noise amplifier (LNA) in the band of 2–4 GHz with a gain of 45 dB (noise factor 0.5 dB) is used to achieve sufficient gain. A variable attenuator with a dynamic range of 70 dB is used to control the IF power of IF input signal.

4.6. Preliminary results

The chest displacement varies between 4 and 12 mm due to respiration, while it ranges between 0.2 and 0.5 mm due to heart beating [19]. The measurement of this small displacement is the objective of this work. The variation of the phase of S_{21} is directly proportional to the chest displacement and indirectly proportional to the wavelength of the signal according to the following relationship:

$$\Delta\theta(t) = \frac{4\pi\Delta x(t)}{\lambda} \tag{3}$$

where λ is the wavelength of the transmitted signal and Δ is the chest displacement.

In order to validate the proposed system, measurements were performed at different frequencies. This section describes the measurements setup. As the frequency range of the antenna is between 2 and 18 GHz, and the maximum frequency of the VNA is 20 GHz, a set of experiments were performed between 2 and 18 GHz. Specifically, experiments were performed at 2.4, 5.8, 10, and 16 GHz. Another operational frequency, 60 GHz, was used via up- and down-conversion methods between 3.5 and 60 GHz. These two versions of the system were tested with a total output power of −10 dBm and for a distance of 1 m between the antennas and the person. The total output power, in other words radiated power, is the transmitted power added to the gain of the antenna. Measurements were performed on a 27-year-old healthy person, while holding the breath for a duration of 10 s [50]. The number of points taken for this window of time is 20,000 points. Hence, a sampling frequency of 2 kHz is obtained.

Performing a measurement begins by generating a continuous wave signal at the desired operational frequency. This CW signal, generated by the VNA, is driven to the transmitting antenna that is directed to the subject's chest. Reflected off the chest of the person under test, the signal is received by the receiving antenna and is driven back to the VNA. The phase variation S_{21}, which corresponds to the difference in terms of phase between the transmitted and the received signal, is computed. The difference in phase is due to the chest displacement. Hence, it contains information about the cardiopulmonary signals when breathing normally and about the heartbeat signal when holding the breath.

The theoretical values of the phase variation due to the chest displacement ranges and the average phase variation obtained by measurements when operating at 2.4, 5.8, 10, 16, and 60 GHz are shown in **Table 1**.

Frequency	Wavelength (λ)	$\Delta\theta$ for Δx = 0.2 mm	$\Delta\theta$ for Δx = 0.5 mm	Experimental $\Delta\theta$
2.4 GHz	125 mm	1.15°	2.88°	1.57°
5.8 GHz	51.72 mm	2.78°	6.96°	3.66°
10 GHz	30 mm	4.8°	12°	5.27°
16 GHz	18.75 mm	7.68°	19.2°	10.46°
60 GHz	5 mm	28.8°	72°	43.85°

Table 1. Theoretical and measured phase variations due to chest displacement.

For each of the utilized frequencies, the phase variation ranges within the theoretical limits. **Figure 2** shows the phase variations due to heartbeat signals detected at different frequencies and plotted within the same scale. It can be noticed that the phase variation increases when
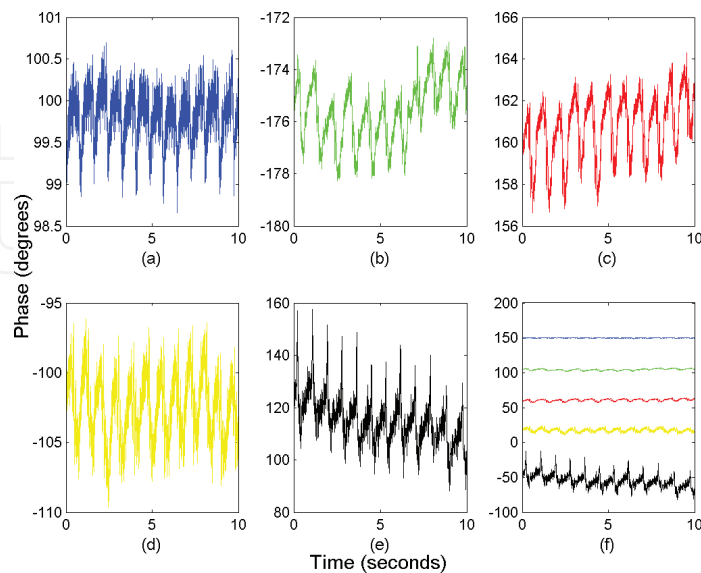

Figure 2. Phase variation of S_{21} due to heartbeat signal measured when holding the breath at different operational frequencies: (a) 2.4 GHz, (b) 5.8 GHz, (c) 10 GHz, (d) 16 GHz, (e) 60 GHz, and (f) all frequencies over the same scaling.

the frequency increases. Thus, higher sensitivity to small displacements is obtained at higher frequencies. The use of higher frequencies will reduce the noise effect and increase the accuracy in detecting the peaks of the signal.

5. Cardiopulmonary signals at different sides: front, back, left, and right

As the cardiopulmonary monitoring for patients and people under rubble requires heartbeat detection regardless their positions with respect to the system, measurements were performed at the four different sides from the PUT: front, back, left, and right. This section describes the measurement and shows the results of the contactless cardiopulmonary detection at four different sides.

5.1. Measurement setup

The measurements were performed on a 54-year-old healthy subject, sitting at a distance of 1 m from the antennas. The operational frequency of the microwave system is 5.8 GHz with a total output power of 0 dBm. Each measurement lasts 30 s where the PUT breathes normally. The contactless measurement signal is acquired simultaneously with a PC-based ECG to be used as a reference signal for the heartbeat detection in order to validate the accuracy of both the microwave system and the signal processing technique. **Figure 3** presents the phase of S_{21} measured at four positions: (a) measurement from the front side of the person, (b) measurement from the back side of the person, (c) measurement from the left side of the person, and (d) measurement from the right side of the person.
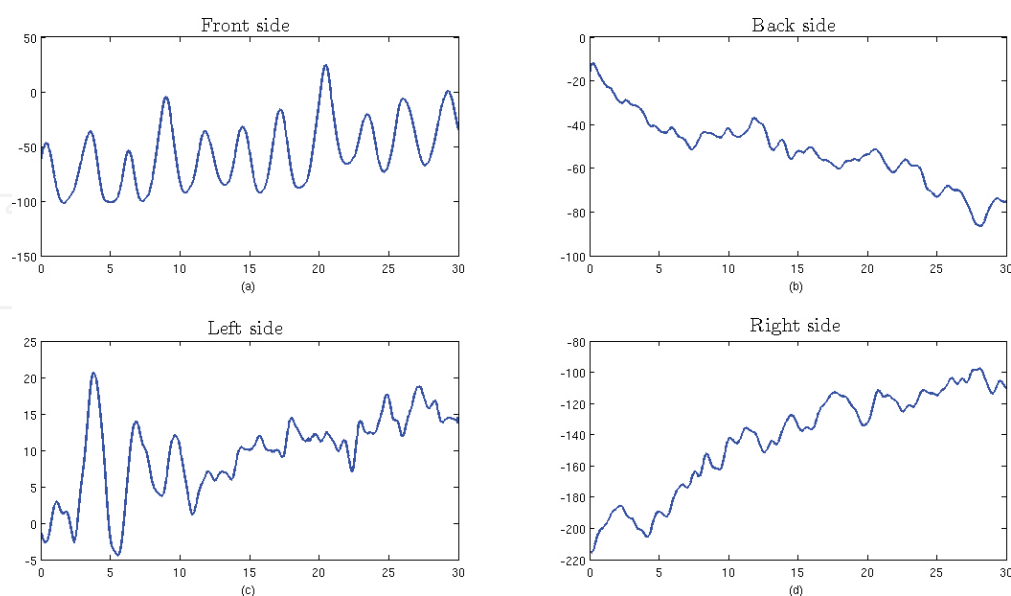

Figure 3. Phase variation of S_{21} due to the cardiopulmonary activities measurement at different sides from the subject: (a) front side, (b) back side, (c) left side, and (d) right side.

It can be noticed that the respiration signal is from the front side of the subject is clearer than other sides in time domain. The signal processing technique in the next subsection will show how it is possible to extract the heartbeat signal from the cardiopulmonary signal over all sides.

5.2. Signal processing techniques

Because the phase variations of S_{21} caused by respiration are larger than those caused by the heart beating, processing techniques are required to extract heartbeat signal from the obtained cardiopulmonary signal. Previous works tend to apply the FFT in order to extract the heartbeat rate. This gives an average value of the HR over a specific window of time; hence, it lacks providing information about the variation of the HR in time and cannot be established in real time as it needs a long-duration window. In order to overcome these problems, the discrete wavelet transform (DWT) is applied to extract the heartbeat signal.

The DWT (W_j, k) of a signal $f(t)$ is given by the scalar product of $f(t)$ with the scaling function (i.e. the wavelet basis function $\phi(t)$ which is scaled and shifted:

$$(W_j, k) \tag{4}$$

where the basis function is given by

$$\phi_j, k(t) = 2^{\frac{-j}{2}} \phi(2^{-j} t - k) \tag{5}$$

where j is the jth decomposition level or step and k is the kth wavelet coefficient at the jth level [51]. DWT is computed by successive low-pass and high-pass filtering of the discrete time-domain signal [51]. DWT determination examines the signal at different frequency bands with different resolutions by decomposing the signal into approximation coefficients (A) and detailed information (D). Hence, this algorithm gives precise analysis of frequency domain at low frequency and time domain at high frequency. The DWT principle is resumed in **Figure 4**.

In general, Dn contains frequencies between $fs/2^n$ and $fs/2^{n+1}$. As the HR varies between 60 and 120 beats per minute, the frequency of the heartbeat is located between 1 and 2 Hz. For the actual sampling frequency used in the VNA (666.7 Hz), no decomposition provides the signal having its frequency component between 1 and 2 Hz. Hence, a re-sampling is needed in order to convert the sampling frequency from 666.7 to 512 Hz. This lets the 1–2 Hz components be included in the 8th-level decomposition of the wavelet. Once the wavelet decomposition is extracted, the signal is reconstructed in time domain, and a peak detection method can be applied in order to detect peaks (beats), thus, to extract the heartbeat rate. The wavelet transform used in this study is the Bior2.4.
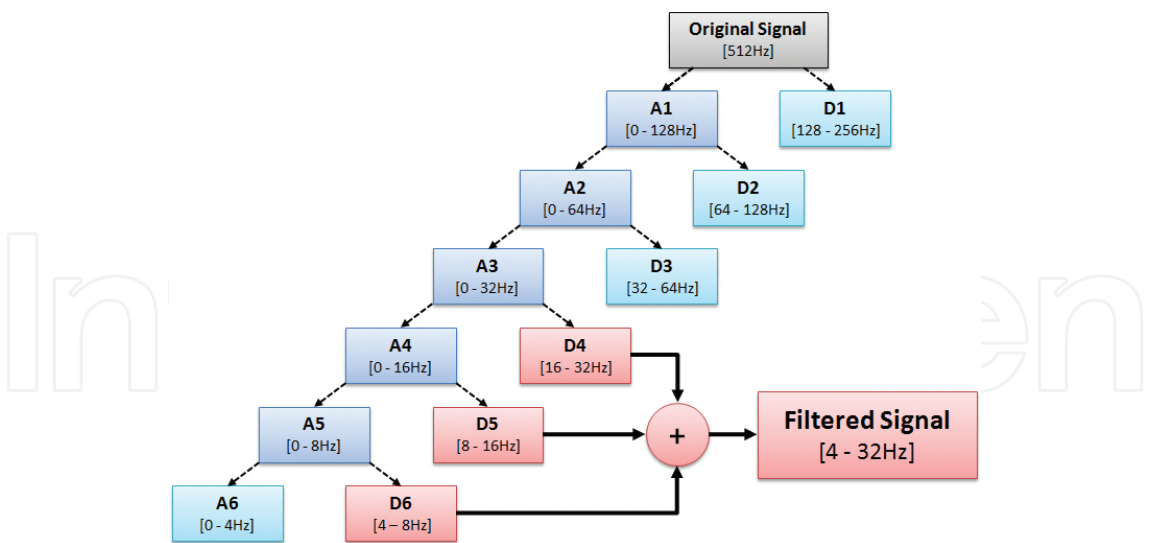
Figure 4. Example of wavelet decomposition.

Figure 5 shows the result of the 8th-level decomposition upon applying Bior2.4 to the cardiopulmonary signal detected from the front side of the PUT as well as the ECG signal extracted simultaneously with the cardiopulmonary signal.
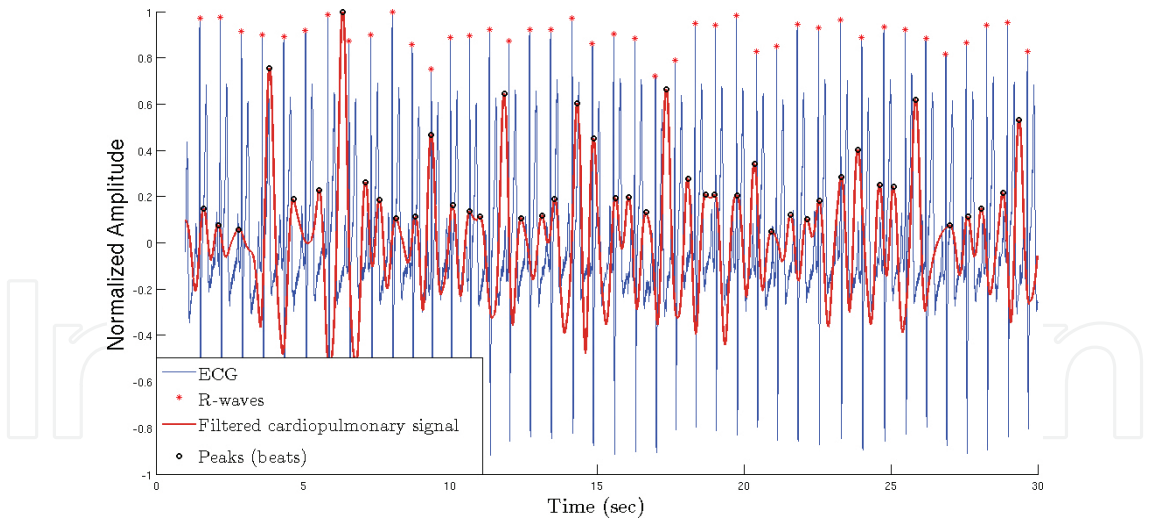

Figure 5. ECG vs. cardiopulmonary signal extracted from the front side of the subject and processed using DWT Bior2.4 level 8.

Applying the peak detection method to both ECG and filtered cardiopulmonary signal detected at the front side from the subject gives, respectively, 41 R-waves and 44 peaks. This results in an HR of 85 bpm for the ECG and 93 bpm for the filtered cardiopulmonary signal.

The result of the 8th-level decomposition upon applying Bior2.4 to the cardiopulmonary signal detected from the back side of the PUT is shown in **Figure 6**.
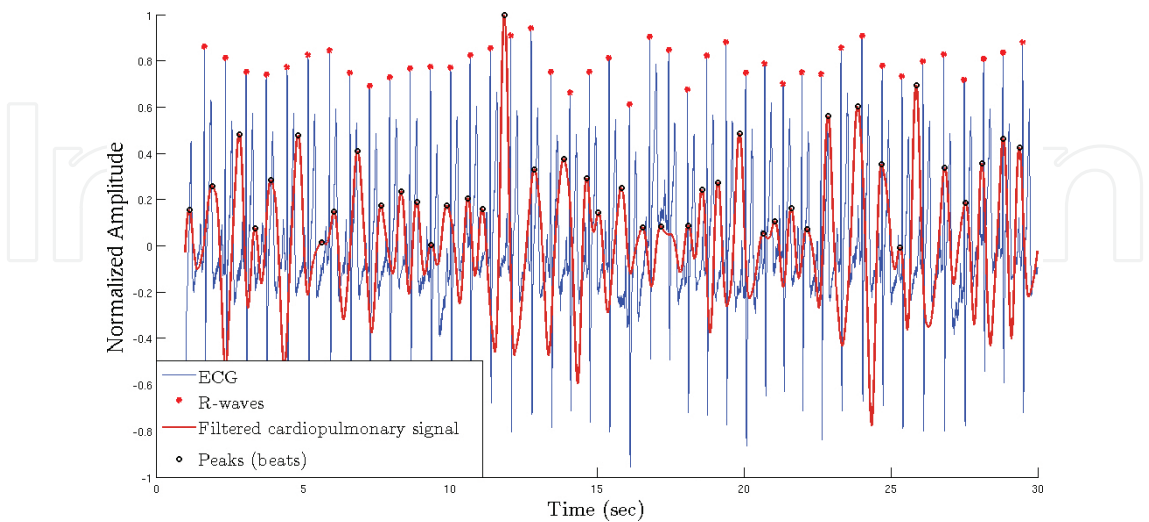

Figure 6. ECG vs. cardiopulmonary signal extracted from the back side of the subject and processed using DWT Bior2.4 level 8.

Applying the peak detection method to both ECG and filtered cardiopulmonary signal detected at the back side from the subject gives, respectively, 42 R-waves and 42 peaks for both signals. This results in an HR of 88 bpm for the ECG and 87 bpm for the filtered cardiopulmonary signal.

The result of the 8th-level decomposition upon applying Bior2.4 to the cardiopulmonary signal detected from the left side of the PUT is shown in **Figure 7**.
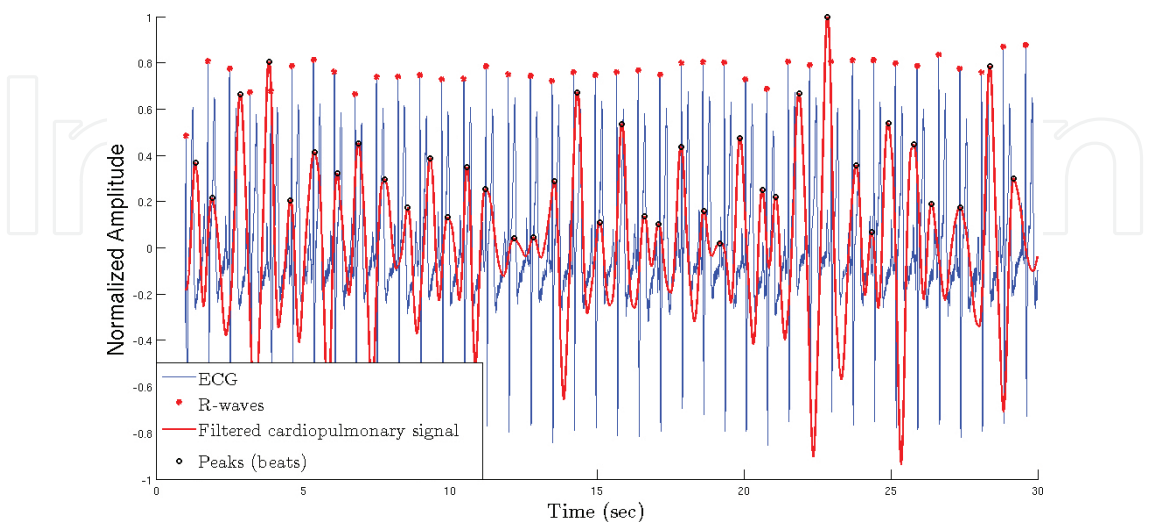

Figure 7. ECG vs. cardiopulmonary signal extracted from the left side of the subject and processed using DWT Bior2.4 level 8.

Applying the peak detection method to both ECG and filtered cardiopulmonary signal detected at the left side from the subject gives, respectively, 40 R-waves and 38 peaks. This results in an HR of 82 bpm for the ECG and 80 bpm for the filtered cardiopulmonary signal.

The result of the 8th-level decomposition upon applying Bior2.4 to the cardiopulmonary signal detected from the right side of the PUT is shown in **Figure 8**.
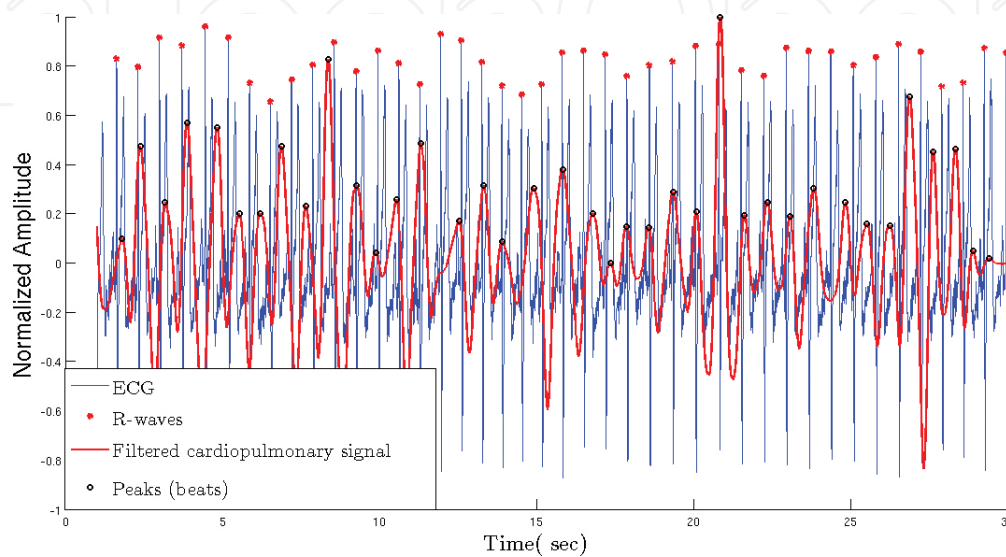

Figure 8. ECG vs. cardiopulmonary signal extracted from the right side of the subject and processed using DWT Bior2.4 level 8.

Applying the peak detection method to both ECG and filtered cardiopulmonary signal detected at the right side from the subject gives, respectively, 42 R-waves and 38 peaks. This results in an HR of 87 bpm for the ECG and 80 bpm for the filtered cardiopulmonary signal.

5.3. Results and discussion

Compared to the HR extracted from the ECG signal, the DWT with Bior2.4 family at decomposition level 8 shows accurate heartbeat detection. The signal processing technique applied to the signal extracted from the front side of the subject shows an error of 9%, while an error of 1% is obtained from the signal extracted at the back side of the subject. Also, the DWT applied to the signal extracted from the left side shows an error of 3% while an error of 7% is obtained for the signal extracted from the right side. **Table 2** shows the results in terms of HR calculation for both ECG and filtered cardiopulmonary signal for the four sides' measurements.

The heartbeat rate for both the ECG and VNA signals are calculated as follows:

$$HR = \frac{60(N-1)}{d_1 + d_2 + ... + d_{N-1}} \tag{6}$$

where N is the number of peaks and d_k is duration between two consecutive peaks. The peaks are detected using a classical peak-detection algorithm that is applied to both the ECG signal and the filtered cardiopulmonary signal.

Measurement side	Heartbeat rate for ECG signal (bpm)	Heartbeat rate for filtered cardiopulmonary signal (bpm)	Absolute relative error (%)
Front	85	93	9.12
Back	88	87	1.43
Left	82	80	2.66
Right	87	80	7.38

Table 2. HR calculation for ECG and filtered cardiopulmonary signals and the obtained relative error.

The relative error of the HR is calculated as

$$Error = \frac{100 * |HR_{ECG} - HR_{VNA}|}{HR_{ECG}} \tag{7}$$

As shown in Section 5.1, the cardiopulmonary signal detected from the front side of the subject shows clear respiration signal in time-domain while other sides' signals do not. On the other hand, when applying the Bior2.4 family of the discrete wavelet transform to the cardiopulmonary signals, the highest accuracy in terms of heartbeat rate is obtained at the back side while the front side shows the lowest accuracy. This is due to the fact that chest displacement due to breathing is higher at the front side than other sides; hence, the chest displacement due to heart beating will be less affected by the respiration signal on other sides.

6. Conclusion

A microwave system used in order to detect the chest wall motion that contains information about respiration and heart beating is described. The system is tested at different operational frequencies: 2.4, 5.8, 10, 16, and 60 GHz on a subject at 1 m from the system while holding the breath for 10 s. Other measurements were performed at 5.8 GHz for different positions for the subject: front, back, left, and right sides. The first measurement is performed on a 27-year-old subject while holding the breath, while the second measurement is performed on a 54-year-old subject while breathing normally. Along with a PC-based ECG, measurements are performed with 0 dBm output power and for a duration of 30 s where the subject breathes normally. The proposed system shows the ability of detecting cardiopulmonary signals for the four sides' positioning: front, back, left, and right. Wavelet transformation is used in processing cardiopulmonary signals in order to extract the heartbeat signal. The 8th-level decomposition of Bior2.4 shows high performance in providing the heartbeat signal in time domain where

high accuracy is obtained in terms of heartbeat rate. A peak detection method is applied to the reconstructed signal from the 8th-level Bior2.4 decomposition. Accuracy in terms of HR for different positions varies between 1% (from the back side) and 9% (from the front side). The proposed system and signal processing technique show the possibility of measuring the cardiopulmonary activities of the subject at four different positions with high accuracy. Compared to other studies, the proposed processing technique shows the ability of detecting the heartbeat signal in time domain, hence, giving information about the variation of the heartbeat rate in real time with an error less than 10%. Future work will concern performing measurements on persons with different ages and under different breathing circumstances as well as for persons in motion.

Author details

Dany Obeid[1*], Sarah Samad[2], Sawsan Sadek[2], Gheorghe Zaharia[1] and Ghaïs El Zein[1]

*Address all correspondence to: dany.obeid@gmail.com

1 IETR UMR 6164, INSA Rennes, Rennes, France

2 University Institute of Technology, Lebanese University, Saida, Lebanon

References

[1] E. Braunwald and J. K. Perlkoff, Physical Examination of the Heart and Circulation, ser. Heart Disease: A Textbook of Cardiovascular Medicine, 2001.

[2] W. Dressler, Pulsations of the chest wall, 1937.

[3] P. M. S. Gillam, A. A. Deliyannis, and J. P. D. Mounsey, The left parasternal impulse, 1964.

[4] E. H. Awtry and J. Loscalzo, Evaluation of the Patient with Cardiovascular Disease, 2001.

[5] A. A. Deliyannis, P. M. S. Gillam, J. P. D. Mounsey, and R. E. Steiner, Thecardiac impulse and the motion of the heart, 1964.

[6] A. E. Aubert, L. Welkenhuysen, J. Montald, L. de Wolf, H. Geivers, J. Minten, H. Kesteloot, and H. Geest, Laser method for recording displacement of the heart and chest wall, 1984.

[7] C. M. Brandt, H. Annoni, J. Harthong, J. M. Reiner, and R. Krauskhopff, Evaluation of chest wall distortion related to cardiac activity by structured lights: A study of the apical impulse by the moiré technique, 1986.

[8]   G. Ramachandran and M. Singh, Three-dimensional reconstruction of cardiac displacement patterns on the chest wall during the p, qrs, and t-segments of the ECG by laser speckle interferometry, 1989.

[9]   G. Ramachandran, S. Swarnamani, and M. Singh, Reconstruction of out-of-plane cardiac displacement patterns as observed on the chest wall during various phases of ECG by capacitance transducer, 1991.

[10] K. Mohri, T. Jinnouchi, and K. Kawano, Accurate mechanocardiogram sensors using amorphous star-shaped core multivibrator combined with a magnet, 1987.

[11] K. Ikegaya, N. Suzumura, and T. Funada, Absolute calibration of phonocardiographic microphones and measurements of chest wall vibration, 1971.

[12] G. W. Yip, Y. Zhang, P. Y. Tan, M. Wang, P. Y. Ho, L. A. Brodin, and J. E. Sanderson, Left ventricular long-axis changes in early diastole: impact of systolic function on diastole, 2002.

[13] A. Owen, Effect of increasing age on diastolic motion of the left ventricular atrioventricular plane in normal subjects, 1999.

[14] O. X. Arcem, O. A. Knudson, M. C. Ellison, P. Baselga, D. D. Ivy, C. DeGroff, and L. Valdes-Cruz, Longitudinal motion of the atrioventricular annuli in children: reference values, growth-related changes, and effects of right ventricular volume and pressure overload, 2002.

[15] T. Kawasaki, S. Sasayama, S. I. Yagi, and T. A. T. Hirai, Non-invasive assessment of the age related changes in stiffness of major branches of the human arteries, 1987.

[16] J. M. Meinders and A. P. G. Hoeks, Simultaneous assessment of diameter and pressure waveforms in the carotid artery, 2004.

[17] T. Kondo, I. Kobayashi, Y. Taguchi, Y. Ohta, and N. Yanagimachi, Adynamic analysis of chest wall motions with MRI in healthy young subjects, 2000.

[18] T. A. Wilson, K. Rehder, S. Krayer, A. Hoffman, C. G. Whitney, and J. R. Rodarte, Geometry and respiratory displacement of human ribs, 1987.

[19] A. DeGroote, M. Wantier, G. Cheron, M. Estenne, and M. Pavia, Chest wall motion during tidal breathing, 1997.

[20] T. Kondo, T. Uhlig, P. Pemberton, and P. D. Sly, Laser monitoring of chest wall displacement, 1997.

[21] J. C. Lin, Non-invasive microwave measurement of respiration, 1975.

[22] K. H. Chan and J. C. Lin, Microprocessor-based cardiopulmonary rate monitor, 1987.

[23] H. R. Chuang, Y. F. Chen, and K. M. Chen, Microprocessor controlled automatic clutter-cancellation circuits for microwave systems to sense physiological movements remotely through the rubble, 1990.

[24] E. F. Greneker, Radar sensing of heartbeat and respiration at a distance with applications of the technology, 1997.

[25] K. M. Chen, Y. Huang, J. Zhang, and A. Norman, Microwave life-detection systems for searching human subjects under earthquake rubble or behind barrier, 2000.

[26] I. Arai, Survivor search radar system for persons trapped under earthquake rubble, 2001.

[27] A. D. Droitcour, O. B. Lubecke, V. M. Lubecke, and J. Lin, 0.25 μm CMOS and BiCMOS single chip direct conversion Doppler radars for remote sensing of vital signs, 2002.

[28] O. B. Lubecke, G. Awater, and V. M. Lubecke, Wireless LAN PC card sensing of vital signs, 2003.

[29] IEEE Standard for Safety Levels with Respect to Human Exposure to Radio Frequency Electromagnetic Fields, 3 kHz to 300 GHz Amendment 2: Specific Absorption Rate (SAR) Limits for the Pinna, 2004.

[30] Y. Xiao, J. Lin, O. B. Lubecke, and V. M. Lubecke, A ka-band low power Doppler radar system for remote detection of cardiopulmonary motion, 2005.

[31] Q. Zhou, J. Liu, A. H. Madsen, O. B. Lubecke, and V. Lubecke, Detection of multiple heartbeats using Doppler radar, 2006.

[32] O. B. Lubecke, V. Lubecke, A. Host-Madsen, D. Samardzija, and K. Cheung, Doppler radar sensing of multiple subjects in single and multiple antenna systems, 2005.

[33] V. M. Lubecke, O. B. Lubecke, A. H. Madsen, and A. E. Fathy, Through-the-wall radar life detection and monitoring, 2007.

[34] C. Li and J. Lin, Random body movement cancellation in doppler radar vital sign detection, 2008.

[35] Y. Wang; Q. Liu; A. E. Fathy, CW and pulse–Doppler radar processing based on FPGA for human sensing applications, 2012.

[36] W. Hu, Z. Zhao, Y. Wang, H. Zhang, and F. Lin, Noncontact accurate measurement of cardiopulmonary activity using a compact quadrature Doppler radar sensor, 2013.

[37] C. Li and J. Lin, Complex signal demodulation and random body movement cancellation techniques for non-contact vital sign detection, 2008.

[38] D. L. Gorgas, Vital Signs and Patient Monitoring Techniques, 2004.

[39] V. Lubecke, O. B. Lubecke, and E. Beck, A compact low-cost add-on module for Doppler radar sensing of vital signs using a wireless communications terminal, 2002.

[40] B. Lohman, O. B. Lubecke, V. Lubecke, P. Ong, and M. Sondhi, A digital signal processor for Doppler radar sensing of vital signs, 2002.

[41] C. Li, Y. Xiao, and J. Lin, Experiment and spectral analysis of a low-power ka-band heartbeat detector measuring from four sides of a human body, 2006.

[42] J. Li, L. Liu, Z. Zeng, and F. Liu, Advanced signal processing for vital sign extraction with applications in UWB radar detection of trapped victims in complex environments. IEEE Journal of Selected Topics in Applied Earth Observations and Remote Sensing. 2013;7(3):783–791.

[43] H. Zhang; S. Li ;X. Jing ;P. Zhang ;Y. Zhang, T. Jiao, G. Lu, J. Wang, The separation of the heartbeat and respiratory signal of a Doppler radar based on the LMS adaptive harmonic cancellation algorithm, 2013.

[44] M. K. Singh, A. Gupta, S. Permanand, U. Singh, O. P. Singh, Y. H. Kim, A. K. Singh, System modeling and signal processing of microwave Doppler radar for cardiopulmonary sensing, 2015.

[45] J. Tu, J. Lin, Fast acquisition of heart rate in noncontact vital sign radar measurement using time window-variation technique, 2015.

[46] IEEE Standard for Safety Levels with Respect to Human Exposure to Radio Frequency Electromagnetic Fields, 3 kHz to 300 GHz, 1992.

[47] J. C. Lin, Safety standards for human exposure to radio frequency radiation and their biological rationale, 2003.

[48] Biological effects and exposure criteria for radio frequency electromagnetic fields, 1986.

[49] D. Obeid, S. Sadek, G. Zaharia, and G. El-Zein, Non-contact heart-beat detection at 2.4, 5.8 and 60 GHz: a comparative study, 2009.

[50] D. Obeid, G. Zaharia, S. Sadek, G. El Zein, Microwave Doppler radar for heartbeat detection vs electrocardiogram, 2012.

[51] G. Alan Blackburn, J. Garke Ferwerda, Retrieval of chlorophyll concentration from leaf reflectance spectra using wavelet analysis, 2007.

[52] A. Ronaszeki, A. E. Aubert, and H. de Geest, Laser apexcardiogram in healthy young men: A comparative study with the conventional method, 1990.

[53] M. Singh and G. Ramachandran, Reconstruction of sequential cardiac inplane displacement patterns on the chest wall by laser speckle interferometry, 1991.

[54] K. Mohri, T. Kondo, H. Sugino, J. Yamasaki, and K. Yoshino, Non-contact linear displacement sensors using amorphous-core multivibrators for mechanocardiography, 1985.

[55] J. Lin, J. Kiernicki, M. Kiernicki, and P. Wollschlaeger, Microwave apexcardiography, 1979.

[56] Y. Xiao, J. Lin, Boric-Lubecke, and V. M. Lubecke, Frequency tuning technique for remote detection of heartbeat and respiration using low-power double-sided and transmission in ka-band, 2006.

[57] J. C. Lin, E. Dawe, and J. Majcherek, A noninvasive microwave apnea detector, 1977.

[58] H. R. Chuang, Y. F. Chen, and K. M. Chen, Automatic clutter-canceler for microwave life-detection systems, 1991.

[59] C. Li, J. Lin, and Y. Xiao, Robust overnight monitoring of human vital signs by a noncontact respiration and heartbeat detector, 2006.

[60] Guidelines for limiting exposure to time-varying electric, magnetic and electromagnetic fields (up to 300 GHz), 1998.

[61] J. M. Osepchuk and R. C. Petersen, Historical review of RF exposure standards and the international committee on electromagnetic safety (ICES), 2003.

[62] D. Obeid, S. Sadek, G. Zaharia, and G. El Zein, Multitunable microwave system for touchless heartbeat detection and heart rate variability extraction, 2010.